Optimizing GRACE/GRACE-FO data and *a priori* hydrological knowledge for improved global Terrestial Water Storage component estimates

Natthachet Tangdamrongsub [a,b], Cheinway Hwang [c], Jordan S. Borak [a,b], Saowanit Prabnakorn [d], and Jiancheng Han [c]

[a] Earth System Science Interdisciplinary Center, University of Maryland, College Park, Maryland, USA

[b] Hydrological Sciences Laboratory, NASA Goddard Space Flight Center, Greenbelt, Maryland, USA

[c] Department of Civil Engineering, National Chiao Tung University, Hsinchu, Taiwan

[d] Agricultural Engineering, Faculty of Engineering, Rajamangala University of Technology Thanyaburi, Thailand

Correspondence to: natthachet.tangdamrongsub@nasa.gov

Abstract

The comprehensive information of global terrestrial water storage (TWS) components (soil moisture, groundwater, snow, surface water) is essential for effective assessment of water resource availability, climate variation, and disaster mitigation measures. Observational data provided by the Gravity Recovery And Climate Experiment (GRACE) and GRACE Follow-On satellite missions offer global TWS variation (ΔTWS) in terms of an integrated water column. However, GRACE spatial resolution is relatively coarse (i.e., 3°), and the vertically integrated value cannot be separated into ΔTWS components directly. This study demonstrates the feasibility to estimate ΔTWS components at any desired spatial-vertical resolution by effectively maintaining the native resolution of the employed hydrological knowledge. It utilizes a least-squares with constraints (LSC) approach to rigorously incorporate GRACE and GRACE-FO data and *a priori* hydrological knowledge, with the aim to improve global ΔTWS components' accuracy and spatial resolution. The 3°×3° GRACE mascon derived ΔTWS data is disaggregated into the 0.5°×0.5° anomalous soil moisture storage (ΔSMS), groundwater storage (ΔGWS), snow water equivalent (ΔSWE), and surface water storage (ΔSWS) based on the covariance information obtained from the Community Atmosphere Biosphere Land Exchange (CABLE) and the PCRaster Global Water Balance (PCR-GLOBWB) models. Evaluation with different ground measurements and satellite products between 2002 and 2019 exhibits significantly improved accuracy in all individual ΔTWS components. This improvement is of particular note in ΔGWS and ΔSWS, where the LSC approach increases the globally averaged correlation values by approximately 0.13 and 0.05, respectively. Reliable prior knowledge leads to a more accurate ΔTWS component estimate, and the use of ensemble-mean knowledge yields the best result.

Keywords: GRACE, GRACE-FO, Least-squares with constraints, TWS component, *a priori* hydrological knowledge, spatial resolution

1. Introduction

Terrestrial hydrological mass variation is a fundamental component of the Earth's climate system (Huntington 2006; Tapley et al., 2019). Annual or interannual terrestrial mass change is attributed to the variation of terrestrial water storage (ΔTWS), and its accurate measurement is required for reliable assessment of water resources management, climate variation, and disaster mitigation measures (Haddeland et al., 2014). In fact, the importance of TWS measurement is acknowledged in the recent 2018 Decadal Report (NASEM, 2018). TWS comprises multiple storage components, e.g., soil moisture storage (SMS), snow water equivalent (SWE), groundwater storage (GWS), and surface water storage (SWS). Satellite-borne observation of TWS components has provided significant benefits to scientific and industrial sectors (e.g., Derksen et al., 2010; McNairn et al., 2012).

Measuring comprehensive TWS components from space is challenging, considering satellite sensors' limited sensitivity (e.g., Crow et al., 2012). For example, the satellite soil moisture sensor is only sensitive to the mass variation in the top 2 – 5 cm soil layer (e.g., Entekhabi et al., 2010), while the dominant components of TWS are located at much deeper layers (e.g., root zone soil moisture, groundwater). Similarly, a satellite imaging sensor can be used to derive the surface water component (e.g., Mueller et al., 2016), but the observation does not contain depth information that can be used to obtain the surface water mass variation. Meanwhile, the only valid measurement of Earth's mass variation is the integrated water storage (i.e., ΔTWS) derived from gravity observations provided by the Gravity Recovery And Climate Experiment (GRACE; Tapley et al., 2004) and GRACE follow-on missions (Flechtner et al., 2016). For convenience, we use the term GRACE to refer to GRACE or GRACE-FO in this paper.

GRACE is a low-low satellite-to-satellite tracking system flying in a near-polar orbit at approximately 500 km altitude above the Earth's surface (Tapley et al., 2004). The K-band ranging system is used to measure the range (or range rate) deviation between the twin satellites induced by the Earth's gravity change, and this range measurement is used to derive the hydrological mass variation. Due to the nature of satellite architecture and orbit configuration, GRACE is only sensitive to ΔTWS of relatively large areas (e.g., > 90,000 km^2) or mass change greater than ~1 Gton (assuming 1 cm equivalent water height in a 3°×3° area). The coarse spatial resolution of GRACE measurement limits its application to ΔTWS studies in large river basins, whereas effective communication with the private sector or public stakeholders would require ΔTWS component information at the local level (Quiring, 2009). An additional limitation is that the vertically integrated mass change cannot be separated into ΔTWS components directly (e.g., Rodell et al., 2009). This motivates us to develop a horizontal-vertical approach to downscaling that enhances the GRACE data's utility – perhaps to its maximum potential.

Successful enhancement in horizontal-vertical scales of GRACE data has been reported in previous studies. For instance, Miro and Famiglietti (2018) exploited spatial details of *in situ* groundwater observations in order to bring the spatial resolution of ΔTWS, and GWS variation (ΔGWS) down to 16 km^2. Yin et al. (2018) adopted a similar concept using remotely sensed evapotranspiration data as a reference. In addition, simple vertical decompositions were given by, e.g., Rodell et al. (2009), Scanlon et al. (2018), and Yin et al. (2020), who extracted the ΔGWS component from GRACE data by removing modeled ΔSMS, ΔSWE, and ΔSWS from GRACE-derived ΔTWS. Andrew et al. (2017) also demonstrated a proof of concept to decompose GRACE data using wavelets. However, it is noteworthy that the previous downscaling studies were specific to one particular region or one ΔTWS component (mostly

ΔGWS), while the enhancement of comprehensive global ΔTWS components has not been considered to date. The availability of such a global product would benefit a broader range of hydrological applications.

One practical approach to enhancing the horizontal-vertical scale and accuracy of ΔTWS components is to employ a statistical optimization between GRACE ΔTWS observations and *a priori* knowledge of ΔTWS components. A similar approach was demonstrated by Tangdamrongsub et al. (2012; 2018), in which the least-squares with constraints (LSC) method was used to disaggregate GRACE observations into individual ΔTWS components based on *a priori* horizontal-vertical detail. In fact, LSC combines the strength of both GRACE observations and *a priori* knowledge to produce high-spatial-resolution ΔTWS components from *a priori* hydrological knowledge, while maintaining accurate ΔTWS magnitude using observations. The required hydrological knowledge in this approach can be obtained from freely accessible hydrological or land surface models (e.g., Rodell et al., 2004; Decker, 2015; Sutanudjaja et al., 2018). The advantages of the LSC approach lay in straightforward implementation, computationally affordability, and exclusive reliance on public domain datasets.

The objectives of this study are twofold:

1) to improve subgrid-level GRACE global ΔTWS component estimates by optimizing the gravity data with reliable hydrological knowledge, and
2) to assess the benefit of GRACE measurements on individual storage layers.

Our computation employs GRACE and GRACE-FO mascon solutions (Wiese et al., 2016) and *a priori* hydrological knowledge from two different models, the PCRaster Global Water Balance (PCR-GLOBWB; Sutanudjaja et al., 2018), and the Community Atmosphere Biosphere Land

Exchange (CABLE; Decker, 2015), to estimate global ΔTWS components at 0.5°×0.5° spatial resolution between April 2002 and December 2019 – consistent with the approximate period of GRACE and GRACE-FO data. The results are evaluated with measurements from different ground data networks (e.g., groundwater networks in India, Australia, China) and various remote sensing products. The Spearman's correlation coefficient (ρ) is used as an evaluation metric to highlight GRACE's benefit in the global ΔTWS components estimate.

2. Data

2.1 GRACE mascon

This study uses the GRACE and GRACE-FO mascon solution (RL06M.MSCNv02) of the Jet Propulsion Laboratory (JPL), California Institute of Technology, obtained from http://grace.jpl.nasa.gov. The mascon approach parameterizes Earth's mass variation using mass concentration blocks as a basis function, which provides a more accurate ΔTWS estimate than that derived from spherical harmonic coefficients (e.g., Rowlands et al., 2010). The JPL mascon product provides monthly ΔTWS variation and uncertainty at ~3° spatial resolution from 2002 to present. Two mascon products are available, (1) the mascon without and (2) with Coastline Resolution Improvement (CRI) filters. The mascon without CRI provides native 3° ΔTWS resolutions, while the mascon with CRI refines ΔTWS near coastal areas to correct for leakage errors. Both solutions adopt the same ΔTWS uncertainty from the mascon without CRI solution. This study uses the mascon without CRI solution to maintain consistency between ΔTWS solutions and the provided uncertainty. The solutions between April 2002 and December 2019 are used in this study. At each mascon cell, the long-term mean computed from all data in time series is removed from each monthly data to obtain ΔTWS relative to our study period.

2.2 *A priori* hydrological knowledge

The *a priori* information of ΔTWS components is obtained from the SubgridSoil GroundWater (CABLE-SSGW; Decker, 2015) and PCR-GLOBWB Version 2 (Sutanudjaja et al., 2018) models. The CABLE model is the land surface model (LSM) of the Australian Community Climate and Earth System Simulator (ACCESS; Bi et al., 2013). CABLE describes the sophisticated atmosphere, biosphere, and hydrosphere processes using five different modules, i.e., radiation, canopy, surface flux, soil, and ecosystem carbon. The water storage components of CABLE can be estimated from the soil, snow, and vegetation routines (see, e.g., Decker, 2015; Tangdamrongsub et al., 2018 for more detail). In this study, CABLE-estimated TWS components include SMS, GWS, and SWE.

PCR-GLOBWB is a grid-based hydrology model that simulates continuous fields of hydrological variables such as water storage, flux, and human water use. PCR-GLOBWB includes surface water and groundwater abstraction controlled by water availabilities and water demands for irrigation, industrial sectors, and households. Both CABLE and PCR-GLOBWB can be used to simulate monthly global ΔTWS components at 0.5°×0.5° spatial resolution. The distinct differences between the two are that PCR-GLOBWB also includes human intervention and ΔSWS components. The new public version of PCR-GLOBWB (Sutanudjaja et al., 2018) extends the time series from 2010 to 2015, but several parameters are still not available during this extended period. PCR-GLOBWB simulations use the most recent information (e.g., domestic/industrial water demand) for the year those parameters are unavailable. For instance, when the parameter is only available up to 2012, the 2012 parameter will be used for 2013 and beyond. Complete model descriptions of CABLE and PCR-GLOBWB can be found in Decker (2015) and Sutanudjaja et al. (2018), respectively.

In this study, CABLE is forced with the 3-hourly forcing data from the Global Land Data Assimilation System (GLDAS; Rodell et al., 2004). The forcing data include precipitation, air temperature, radiation, wind, and humidity. PCR-GLOBWB is forced with global daily precipitation and temperature data from the European Centre for Medium-Range Weather Forecasts ReAnalysis Version 5 (ERA5) products (Hersbach and Dee, 2016). These forcing data are selected based on (1) a global (or near global) coverage, (2) an extended time span covering our study period, and (3) effective simulation performance seen from previous studies (e.g., Tangdamrongsub et al., 2018; Tangdamrongsub and Šprlák, 2021). Note that the daily total precipitation and mean temperature in this paper are resampled from the hourly data of ERA5. The daily potential evapotranspiration is calculated using the Hamon method (Lu et al., 2005). Both forcing datasets are down-sampled (averaged) from a 0.25°×0.25°grid to a 0.5°×0.5° grid, which is consistent with the model grid size. Monthly-averaged ΔTWS components are then computed between April 2002 and December 2019. Similar to the GRACE data, at each model grid cell, the variations of ΔTWS components are computed by subtracting the long-term mean computed from the data over the entire study period.

2.3 Validation data

In situ groundwater data are obtained from groundwater networks in five different regions (Table 1). The *in situ* data are provided in terms of groundwater level variation (ΔH) with respect to a given datum or other vertical reference. The ΔH time series is available at an hourly or daily interval in most regions except India, where only a seasonal time step (i.e., four times per year) is provided. Only groundwater level sites with records available between 2002 and 2019, and missing less than 36 months of observations are used in the validation. The conversion from groundwater level to groundwater storage is not performed due to our limited knowledge of accurate specific yield value.

Altimeter-based water level measurements are used to evaluate the ΔSWS estimate. The products are acquired from the United States Department of Agriculture, Global Reservoirs and Lakes Monitor website (USDA G-REALM; https://ipad.fas.usda.gov/cropexplorer/global_reservoir; last access: 3 June 2020). The Topex/Poseidon, Jason-1, Jason-2/OSTM, and Jason-3 (TPJOJ) product version 2.4 provides smoothed water level variations (ΔL) every ~10-day. Only the measurements that meet the two required conditions are considered in our comparison, (1) the location coincides with the water body of *a priori* knowledge (in this case, ΔSWS can be estimated from the LSC solution), and (2) the ΔL records are available during the evaluation period (April 2002 – December 2019).

The root zone soil moisture and SWE data are obtained from two different remote sensing products, the Soil Moisture Active Passive (SMAP) Level-4 product (Reichle et al., 2017; https://nsidc.org/data/smap/smap-data.html (last access: 20 March 2021)) and the Copernicus Global Land Service (CGLS) SWE product (Luojus et al., 2017b; https://land.copernicus.eu/global/products/swe (last access: 20 March 2021)). The SMAP data provide a near-global 3-hour root zone volumetric soil moisture at ~9 km resolution, available from 2015 to the present. The CGLS SWE data provide daily SWE at ~5 km over the Northern hemisphere, operational since 2006. Both datasets are resampled to a 0.5°×0.5° grid by spatially averaging all data inside each grid cell, as is consistent with the LSC estimates' spatial resolution.

For each validation dataset, the monthly variation time series is computed prior to the validation. Note that, as the TWS component estimates and the data for validation are not always consistent, we used Spearman's correlation coefficient as an evaluation metric to assess the agreement between them. Similar evaluation approaches were adopted in previous studies (e.g., Dorigo et al., 2017; Girotto et al., 2017).

3. Methods

3.1 Least-squares with constraints (LSC) approach

The fine-scale (i.e., 0.5°) ΔTWS components are estimated from least-squares estimation with constraints (Fig. 1). First, the observation equation describing a relationship between the fine-scale ΔTWS components ($\boldsymbol{x}$) and the GRACE mascon estimate ($\boldsymbol{y}$) can be written as follows:

$$\boldsymbol{e} = \mathbf{A}\boldsymbol{x} - \boldsymbol{y};\ \mathbf{C}_{\mathbf{y}}\,, \tag{1}$$

where $\mathbf{A}$ is a design matrix connecting the finer-grid ΔTWS components to the associated mascon, $\boldsymbol{e}$ is a residual vector of the observation equations, and $\mathbf{C}_{\boldsymbol{y}}$ is the covariance matrix of the observations. With given *a priori* values of the ΔTWS components ($\boldsymbol{x}_{\mathbf{0}}$), the constraint equation can be written in a similar way:

$$\boldsymbol{e}_{\boldsymbol{x}} = \boldsymbol{x} - \boldsymbol{x}_{\mathbf{0}};\ \mathbf{C}_{\boldsymbol{x}}\,, \tag{2}$$

where $\boldsymbol{e}_{\boldsymbol{x}}$ is a residual vector of the constraint equations, and $\mathbf{C}_{\boldsymbol{x}}$ is the covariance matrix of $\mathbf{x}_{\mathbf{0}}$. The vector $\boldsymbol{x}$ can then be estimated using least-squares, and the target function ($\phi(\boldsymbol{x})$) to determine $\boldsymbol{x}$ is

$$\phi(\boldsymbol{x}) = \|\mathbf{A}\boldsymbol{x} - \boldsymbol{y}\|_{\mathbf{C}_y}^2 + \lambda^2 \|\boldsymbol{x} - \boldsymbol{x}_\mathbf{0}\|_{\mathbf{C}_x}^2, \tag{3}$$

where λ is a regularization parameter, and $\| \quad \|$ represents the Euclidean norm. By minimizing the target function, we obtain the best and unbiased estimation of $\boldsymbol{x}$ as

$$\hat{\boldsymbol{x}} = \left(\mathbf{A}^T \mathbf{C}_y^{-1} \mathbf{A} + \lambda^2 \mathbf{C}_x^{-1}\right)^{-1} \left(\mathbf{A}^T \mathbf{C}_y^{-1} \boldsymbol{y} + \lambda^2 \mathbf{C}_x^{-1} \boldsymbol{x}_\mathbf{0}\right). \tag{4}$$

Equation 4 suggests that $\hat{\boldsymbol{x}}$ receives the contributions from both observations and *a priori* values of $\boldsymbol{x}$ (i.e., $\boldsymbol{x}_\mathbf{0}$**)** with different weights determined by their respective covariance matrices. When *a priori* information has neglegible weights (e.g., $\mathbf{C}_x$ contains large diagonal elements), Eq. (4) results in least-squares solution without constraints, i.e., $\hat{\mathbf{x}} = \left(\mathbf{A}^\mathbf{T} \mathbf{C}_y^{-1} \mathbf{A}\right)^{-1} \mathbf{A}^\mathbf{T} \mathbf{C}_y^{-1} \boldsymbol{y}$. In this case, the solution uses only the information from the observations. Similarly, the solution is in favor of *a priori* knowledge ($\hat{\boldsymbol{x}} = \boldsymbol{x}_\mathbf{0}$) when the observations have relatively small weights compared the initial information.

[Suggested location of Figure 1]

The λ term is used to achieve a balance between the contributions from observations and *a priori* knowledge. In this paper, we employ an L-curve criterion approach of Hansen and O'Leary (1993) to search for the optimal λ value. In the L-curve approach, the 2-dimensional plot between $\|\mathbf{A}\boldsymbol{x} - \boldsymbol{y}\|_{\mathbf{C}_y}^2$ and $\|\boldsymbol{x} - \boldsymbol{x}_\mathbf{0}\|_{\mathbf{C}_x}^2$ associated with given λ values displays an L-shape curve, and the vertex of the curve is where the optimal λ value produces the required criterion (i.e., minimizing both $\|\mathbf{A}\boldsymbol{x} - \boldsymbol{y}\|_{\mathbf{C}_y}^2$ and $\|\boldsymbol{x} - \boldsymbol{x}_\mathbf{0}\|_{\mathbf{C}_x}^2$). Comprehensive details of the L-curve approach, including software and user guides can be found at http://www2.compute.dtu.dk/~pcha/Regutools (last access: 6 July 2020).

3.2 Implementation

The LSC approach is used to spatially and vertically disaggregate ~3°×3° GRACE mascon ΔTWS into 0.5°×0.5° ΔTWS components. Figure 2 illustrates the concept of the horizontal-vertical disaggregation process. From Eqs. (2 – 4), the vector $\boldsymbol{x}_0$ stores the 0.5°×0.5° model-derived ΔTWS components of all global grid cells:

$$\boldsymbol{x}_0 = \begin{bmatrix} \boldsymbol{x}_{01} \\ \boldsymbol{x}_{02} \\ \boldsymbol{x}_{03} \\ \vdots \\ \boldsymbol{x}_{0N} \end{bmatrix}_{NM\times 1} , \tag{5}$$

$$\boldsymbol{x}_{0i;i=1,N} = \begin{bmatrix} \Delta\mathrm{SMS}_i \\ \Delta\mathrm{GWS}_i \\ \Delta\mathrm{SWE}_i \\ \Delta\mathrm{SWS}_i \end{bmatrix}_{M\times 1} , \tag{6}$$

where $\boldsymbol{x}_{0i}$ contains the ΔTWS components of the grid cell i, and N is the number of total grid cells globally (or regionally). In each 0.5°×0.5° grid cell, the vector $\boldsymbol{x}_{0i}$ consists of M ΔTWS components (i.e., ΔSMS, ΔGWS, ΔSWE, and ΔSWS). The observation vector $\boldsymbol{y}$ is a $K \times 1$ vector containing the GRACE mascon. The design matrix $\mathbf{A}$ is a sparse matrix relating the 0.5°×0.5° ΔTWS components to an associated mascon as follows:

$$\mathbf{A} = \begin{bmatrix} \frac{1}{L_{k=1}} \boldsymbol{a}_{k=1} \\ \frac{1}{L_{k=2}} \boldsymbol{a}_{k=2} \\ \frac{1}{L_{k=3}} \boldsymbol{a}_{k=3} \\ \vdots \\ \frac{1}{L_{k=K}} \boldsymbol{a}_{k=K} \end{bmatrix}_{K\times NM} , \tag{7}$$

where $\boldsymbol{a}_k$ is a row vector containing one where a model grid cell is inside the 3°×3° mascon k, and zero elsewhere. L_k is the total number of model grid cells inside the mascon k. It is seen that the matrix **A** is simply the averaged operator used to upscale the finer-resolution ΔTWS component to the mascon space.

[Suggested location of Figure 2]

The $\mathbf{C}_y$ is a variance matrix obtained from the mascon solution. Note that only variance components are provided with mascon product. The matrix $\mathbf{C}_x$ can be derived empirically based on the modeled ΔTWS components following two steps. First, the empirical covariance function is computed as follows (Tscherning and Rapp, 1974):

$$C(\psi_{c,d}) = \frac{1}{D}\sum_{i,j}^{D} f_c f_d \,, \psi - \frac{\Delta\psi}{2} \leq \psi_{c,d} \leq \psi + \frac{\Delta\psi}{2} \tag{8}$$

where f_c and f_d are the ΔTWS components at two grid points separated by the spherical distance $\psi_{c,d}$, D is a number of data pairs, and $\Delta\psi$ is a considered interval distance. Then, the empirical covariance (Eq. (8)) is least-squares fit by the exponential function to determine the scale (b) and correlation length ($\mathcal{L}$), and the matrix $\mathbf{C}_x$ is formed as follows:

$$\mathbf{C}_x(\psi) = \exp\left(b - \frac{\psi}{\mathcal{L}}\right) \tag{9}$$

Note that, in this study, the correlation length is determined as a spherical distance where $C(\psi = 0)$ is decreased by half. The correlation length can also be used to approximate the LSC solution's spatial resolution (see Sect. 4.1). More details on covariance estimations and program codes can be found in Tscherning and Rapp (1974).

3.3 Experimental design

The performance of ΔTWS component estimates might be sensitive to the selected *a priori* knowledge given that its horizontal-vertical details are used in the LSC approach. In this study, the LSC solutions are associated with three different hydrological knowledge sources: the CABLE model, the PCR-GLOBWB model, and their average (i.e., ensemble mean). For clarity, these solutions are called CABLE-based, PCR-GLOBWB-based, and EnsMean-based, respectively.

In all three study scenarios, the LSC approach is used to estimate three ΔTWS components (*M* = 3), ΔSMS, ΔGWS, and ΔSWE, as they are available from both CABLE and PCR-GLOBWB models (as well as the ensemble-mean model). In this case, the $\boldsymbol{x}_0$ vector (see Eq. (6)) becomes $\boldsymbol{x}_0 = [\Delta\mathrm{SMS} \quad \Delta\mathrm{GWS} \quad \Delta\mathrm{SWE}]^{\boldsymbol{T}}$. Note that the summation of all $\boldsymbol{x}_0$ elements is ΔTWS.

The ΔSWS variable can only be estimated from the PCR-GLOBWB-based solution due to the available surface water component in PCR-GLOBWB. In this special case, the $\boldsymbol{x}_0$ of Eq. (6) is used, and the number of estimated variables is *M* = 4.

4. Results

4.1 Sensitivity analysis of LSC approach

As seen in Sect. 3.1, the LSC approach's performance is likely sensitive to two essential components, i.e., a regularization parameter (λ) and the selected *a priori* knowledge. The regularization parameter (λ) plays an important role in statistically adjusting the contribution between the given knowledge and GRACE data. Figure 3 illustrates the impact of applying different λ values on LSC solutions. An underestimated λ value (e.g., $\lambda/10$; see Fig. 3c – 3d) decreases the contribution of *a priori* knowledge, resulting in the LSC solution closer to the GRACE mascon estimate considering 3°×3° resolution (see Fig. 3d Vs. 3h). By contrast, an overestimated λ value leads to a negligible impact of the GRACE data, and the LSC solution resembles *a priori* knowledge (see Fig. 3e Vs. 3g). As anticipated, the optimal λ value balances contributions of the initial knowledge and GRACE based on their covariances, producing a solution that does not overly favor one particular input (Fig. 3a).

[Suggested location of Figure 3]

Using different *a priori* knowledge also affects the LSC solution as seen in, e.g., annual amplitude and spatial patterns of the ΔTWS estimates (Fig. 4). For example, comparing with the PCR-GLOBWB-based result (Fig. 4c), the CABLE-based solution (Fig. 4b) shows a more substantial ΔTWS annual variation in, e.g., Africa, Australia, South-East Brazil, which are more consistent with the GRACE mascon estimate (Fig. 4a). On the other hand, the PCR-GLOWB-based estimate reflects the GRACE mascon closely in CONUS and several parts of Europe. The EnsMean-based result (Fig. 4d) contains ΔTWS features of both CABLE and PCR-GLOBWB cases and exhibits the highest-overall agreement with the GRACE mascon result. The ensemble-mean model estimate appears to provide the best *a priori* information for the LSC approach.

[Suggested location of Figure 4]

We also investigated the spatial resolution of the LSC solution. The normalized empirical covariance (see Sect. 3.2) computed from the EnsMean-based ΔTWS estimate (Fig. 5) illustrates that the LSC solution has the same spatial resolution as the ensemble mean model (0.5°). The same behavior is also found in the CABLE-based and PCR-GLOBWB-based solutions (and across all monthly results), highlighting the LSC approach's effectiveness in maintaining high spatial resolution (from given knowledge). The analysis also suggests the feasibility of downscaling GRACE mascon to a much finer scale (e.g., ~10 km), given an improved spatial resolution of recent model developments (e.g., Sutanudjaja et al., 2018).

[Suggested location of Figure 5]

4.2 Estimation of ∆TWS components

The LSC approach disaggregates GRACE mascon information into three different ∆TWS components, ∆SMS, ∆GWS, and ∆SWE (Fig. 6). The root-mean-square (RMS) value computed along the latitude and longitude axes is used to quantify ∆TWS components' magnitude of the corresponding axis (see vertical and horizontal time series in Fig. 6). Note that Antarctica and Greenland (including the surrounding areas) are excluded from the LSC estimation due to high uncertainties in *a priori* knowledge, given an absence of ice sheet mass balance in the model physics' representation (Decker 2015; Sutanudjaja et al., 2018). It is observed from Fig. 6 that the storage layer's structure, such as the magnitude of a ∆TWS component in ∆TWS, has a significant impact on how the LSC approach disaggregates GRACE information. For example, GRACE information is mostly distributed into the ∆SWE component in high latitude regions where snow mass variation is dominant. This is indicated by the RMS values (see Fig. 6a), where the LSC solution shows distinct increased ∆SWE variations (relative to *a priori* knowledge) in, e.g., Alaska, Patagonia, Severny and Yuzhny Islands, and high mountain Asia regions. Similarly, a significant proportion of ∆TWS is allocated into ∆GWS in heavily irrigated areas (e.g., India, North China Plain, California; Fig. 6b), where groundwater is a major component of the mass variation (e.g., Girotto et al. 2017; Scanlon et al., 2018).

[Suggested location of Figure 6]

Figure 7 illustrates the temporal variations of the basin averaged ΔTWS components obtained from ten river basins (see basin boundaries in Fig. 6a) between 2002 and 2019. In most basins, the seasonal variation of ΔTWS is mainly governed by ΔSMS (see also Fig. S1). A phase delay of a few months observed in ΔGWS (compared to ΔSMS; e.g., Fig. 7b, 7d, S1b, S1d) is simply associated with vertical redistribution that can take several months as water moves from the surface to deeper stores. The negative trend of GRACE mascon corresponds to groundwater depletion, particularly in areas affected by human intervention like North West India and the North China Plain (Fig. 7g, 7i). As expected, the contribution of ΔSWE is insignificant at basin-scale and almost zero in low latitude and tropical regions (e.g., Fig. 7h, 7j, S1h, S1j).

[Suggested location of Figure 7]

4.3. Validation

4.3.1 Groundwater storage

The estimated ΔGWS components are validated with groundwater level measurements, ΔH (Sect. 2.3). Note again that validation here is performed only in terms of temporal correlation due to our limited knowledge of the specific yield required to convert ΔH to ΔGWS. Overall, the LSC solution shows notable agreement with ground measurements, with a Spearman's correlation coefficient greater than 0.5 in all five regions (see, e.g., the EnsMean-based solution in Fig. 8a). The PCR-GLOBWB-based solution outperforms the CABLE-based solution in most validated regions, likely attributed to effective model parameter calibration and inclusion of a water consumption routine in the PCR-GLOBWB model. This is especially apparent in the Rhine River basin (Sutanudjaja et al., 2011), where the PCR-GLOBWB's accurate parameterization produces a nearly perfect temporal match between the ΔGWS estimate and the measured groundwater level. Inclusion of groundwater abstraction in PCR-GLOBWB also leads to a more accurate ΔGWS estimate in areas under heavy anthropogenic influence, e.g., North West India (Fig. 8d), North China Plain (Fig. 8e).

[Suggested location of Figure 8]

However, the PCR-GLOBWB-based solution is inferior in Victoria, Australia, where the CABLE-based solution's accuracy is superior (Fig. 8f). This outcome is to be expected from CABLE, the core LSM of the Australian climate model, with outstanding performance over Australian regions (e.g., Tangdamrongsub et al., 2018). The drawback with using CABLE in this study is the absence of a human intervention routine, which leads to underestimated groundwater trends in the CABLE-based solution (Fig. 8d, 8e). The EnsMean-based solution exhibits the best overall performance, where the obtained correlation values are intermediate or greater than the PCR-GLOBWB-based or CABLE-based solution estimates.

It is possible that the ΔGWS accuracy solely comes from prior knowledge. As such, we quantify the LSC approach's performance by comparing the ΔGWS estimate with the prior ΔGWS knowledge, and the correlation values associated with different prior knowledge are shown in Table 2. Positive impact of the LSC approach is observed in all regions, where the LSC solution delivers a higher correlation value (by 0.13 on average) regardless of the choice of *a priori* knowledge. Interestingly, the LSC approach increases the correlation value when the model estimate is already very accurate (see, e.g., PCR-GLOBWB in the Rhine River basin). The evaluation informs the LSC approach's effectiveness while highlighting GRACE data's benefit in the ΔGWS improvement.

[Suggested location of Table 2]

4.3.2 Soil moisture and snow water equivalent

The ΔSMS and ΔSWE estimates are compared with the SMAP-derived root zone soil moisture and CGLS-SWE products, respectively. Note that although the satellite data might be prone to systematic biases (e.g., Reichle and Koster, 2004), the use of SMAP and CGLS-SWE products for validation are still valid here given that the products have already been validated against ground measurements during data production (Reichle et al., 2017; Luojus et al., 2017a).

The ΔSMS estimate shows a notable agreement with the SMAP data with a near-globally averaged correlation value of 0.61 (Fig. 9a). Areas of significant agreement (e.g., with correlation value up to 0.9) are observed in, e.g., Western and Eastern U.S., Europe, and India, while relatively low correlation values are detected in regions dominated by irrigation and snowfall. The absence of irrigation schemes in the SMAP Level 4 product (Reichle et al., 2017) likely leads to mismatches between soil moisture data and the LSC solution (with the inclusion of irrigation routine), resulting in low correlations in irrigated areas, e.g., High Plains (USA) and the Middle East. Also, the satellite soil moisture sensor is known to be ineffective for frozen soil conditions (Chan et al., 2016), which might explain the disagreement between LSC and SMAP estimates in snow regions, e.g., high latitude, Alps, and high mountain Asia.

[Suggested location of Figure 9]

A reasonable agreement is also observed in the ΔSWE estimate, with an average correlation value of 0.59 (Fig. 9b). Higher correlation values are seen in high latitude regions, where ΔSWE governs the seasonal variation of ΔTWS. Our result is in line with the CGLS-SWE validation report (Luojus et al., 2017a), where correlation values are shown to increase with increasing latitude (i.e., ranging from 0.57 to 0.68 between 50° N and 70° N). Low correlations in far-eastern Russia or coastal areas of Europe is unclear, but possibly (or partly) due to ineffective snow dynamics associated with the coarse digital elevation model in the 0.5° resolution model (see Sutanudjaja et al., 2018), resulting in underperformance with ΔSWE estimates.

4.3.3 Surface water storage

Using PCR-GLOBWB as prior knowledge allows the ΔSWS component to be estimated from the LSC approach (see Eq. (6)). Figure 10 shows the correlations between the LSC PCR-GLOBWB-based result and the G-REALM lake level (ΔL) over 275 evaluated lakes and reservoirs. The LSC approach delivers a global-average correlation value of 0.4, while higher correlation (with $\rho > 0.5$) is observed in North and South America, India, and Europe (Fig. 10a). Relative to the PCR-GLOBWB ΔSWS estimate, the LSC solution improves the ρ value by up to 0.8, while the globally-averaged improvement is about 0.05 (Fig. 10b). The improvement is observed over 75% of the evaluated lakes. The approach underperforms in Africa and Central Asia, where the PCR-GLOBWB model cannot effectively provide reliable prior knowledge of irrigation practice, groundwater-surface water interaction, and snow/glacial process (e.g., Sutanudjaja et al., 2018). The magnitude and timing of irrigated-water allocation and snow/glacial meltwater can play a crucial role on ΔSWS (Block et al., 2007; Sorg et al., 2012), and utilizing inaccurate *a priori* knowledge in the LSC approach leads to negative impact on the ΔSWS estimate.

[Suggested location of Figure 10]

The ΔSWS and ΔL estimates show consistent annual/interannual variation and long-term trend features (Fig. 11). The LSC ΔSWS estimate also effectively captures some climate-induced signals. For example, effects of the 2010 La Niña are observed in many parts of Asia. The significantly increased rainfall around 2010 – 2012 (La Niña years) leads to increased ΔSWS and flooding in, e.g., Gandhi Sagar Reservoir (Fig. 11g, S2g), Song Hua Lake (Fig. 11i, S2i), and Lake Eildon (Fig. 11j, S2j). Additionally, the dramatically increased ΔSWS of Lake Erie (Fig. 11b) after 2016 corresponds to increased precipitation and unusually cold weather (reduced evaporation) observed then (see Fig. S2b, S3b).

[Suggested location of Figure 11]

Despite its effectiveness in monitoring flood events, the LSC ΔSWS estimate fails to capture some extremely low ΔSWS features, e.g., in Tiga Reservoir (Fig. 11d). It is found that the ΔSWS magnitude of Tiga Reservoir is much smaller than GRACE's sensitivity (see, e.g., Ahmad and Haie, 2018). The ΔL measurement may reflect a local mass variation that cannot be sensed by GRACE, causing mismatches between the ΔSWS and ΔL time series. Conversely, in spite of missing GRACE or GRACE-FO data during the mission transition period (2017 – 2018), the 2018 drought observed in Mosul Reservoir (Fig. 11e) is anticipated to be captured in the ΔSWS estimate due to a significant mass variation of the reservoir (Issa et al., 2013).

Overall, this evaluation benchmarks an advantage of exploiting GRACE data in surface water analyses, and underscores a possible application of using the LSC solution for monitoring lake/reservoir levels in the future at appropriate locations.

5. Discussion

The LSC approach horizontally-vertically downscales the 3°×3° GRACE JPL mascon into much finer scale (0.5°×0.5°) ΔTWS components. The approach employs spatial and vertical information from *a priori* hydrological knowledge as a proxy for approximating the unknown ΔTWS components' distribution inside the 3°×3° GRACE mascon cell. As such, the degree of accuracy inevitably lies in the reliability of *a priori* information, as observed in previous studies (e.g., Peng et al., 2017; Long et al., 2016; Scanlon et al., 2018). The use of different hydrological information leads to different outcomes, and the use of the ensemble mean (blended) information yields the best overall results. Evaluation with various reference datasets confirms the effectiveness of the LSC approach in delivering accurate 0.5°×0.5° ΔTWS components. The benefit of GRACE observation is prominent in ΔGWS and ΔSWS estimates, consistent with the findings in previous GRACE studies (Rodell et al., 2009; Tangdamrongsub et al., 2016; Girotto et al., 2017; Yin et al., 2018).

The LSC approach improves the globally averaged correlation of GWS estimates over a priori knowledge by 0.13 (from 0.67 to 0.8). A small degree of improvement does not reflect ineffective performance of the LSC approach, but it is a result of a priori knowledge having very high accuracy to begin with. Despite different experiment setups, the correlation improvement is in line with globally average value reported by Li et al. (2019).

In the LSC approach, we find that vertical disaggregation performance depends significantly on the completeness of *a priori* knowledge for the ΔTWS components. Inaccurate covariance information (e.g., based on incomplete ΔTWS components in $\boldsymbol{x}_0$) could lead to an incorrect vertical disaggregation of the GRACE mascon. With the absence of a surface water component in $\boldsymbol{x}_0$ vector, the LSC approach may disaggregate GRACE information into ΔSMS (instead of ΔSWS), resulting in the ΔSWS signal contained within the ΔSMS estimate. This error likely occurs in inundated area, e.g., the Amazon river basin, where ΔSWS dominates ΔTWS (e.g., Syed et al., 2005). A similar type of error may also be seen in ΔSWE in glacially active regions, in which the ΔSWE estimate may contain the long-term variation of the glacial signals (e.g., Tamisiea et al., 2007).

One may notice that the LSC approach shares some similarities with GRACE data assimilation (e.g., Girotto et al., 2017; Li et al., 2019), in which the ΔTWS components are relatively updated toward the GRACE observation. In our context where only monthly storage components are of interest, the LSC approach may require much lighter computational cost, as the ensemble model propagation is not required, and the ΔTWS components can be estimated independently (and separately) for a different month. Also, knowledge from different models can be simply applied in the LSC approach (e.g., ensemble-mean model), while performing data assimilation based on multiple models would increase the complexity and risk of introducing bias into the system. However, thorough comparison between the two methods is beyond this study's scope but highly recommended for future analysis.

An advantage of the LSC approach is its utility to accommodate multiple prior information from publicly available databases. The LSC approach can also accomudate a regionally-blended information, where GRACE data can be downscaled based on different prior knowledge in different regions. As seen in this study, using *a priori* knowledge constructed based on CABLE in Australia and PCR-GLOBWB elsewhere could lead to optimized accuracy of global ΔTWS component estimates. Also, with the growth of high-resolution products, e.g., the ~10 km PCR-GLOBWB (Sutanudjaja et al., 2018) and the ~5 km World-Wide Water model (van Dijk et al., 2018), downscaling can be performed at much higher resolution with the only potential challenge being the computation of a larger matrix that increases exponentially with the increased horizontal-vertical resolution.

6. Conclusion

This study presents the LSC approach to compute accurate ΔTWS components at subgrid GRACE resolution by statistically optimizing hydrological information between GRACE data and *a priori* hydrological knowledge obtained from models. The evaluation demonstrates significant value added by the LSC approach in increasing the ΔTWS component estimates' accuracy, particularly in groundwater and surface water components. The LSC approach's accuracy depends on the reliability of the exploited *a priori* information, and the best overall result can be obtained from the utilization of ensemble-mean knowledge. This study establishes a benchmark for downscaling GRACE information to 0.5°×0.5° spatial scale, while illustrating that the computation of ΔTWS components at a finer spatial scale is feasible given the increased availability of advanced high-resolution hydrological products.

Author contributions

NT: conceptualization, methodology, software, validation, formal analysis, writing original paper, CH, JB, and JH: editted paper, SP: research discussion.

Acknowledgment

NT. was supported by the NASA Earth Science Division in support of the National Climate Assessment.

References

Ahmad, M.T., Haie, N., 2018. Assessing the Impacts of Population Growth and Climate Change on Performance of Water Use Systems and Water Allocation in Kano River Basin, Nigeria. Water 10, 1766. https://doi.org/10.3390/w10121766

Bi, D., Dix, M., Marsland, S., O'Farrell, S., Rashid, H., Uotila, P., Hirst, T., Kowalczyk, E., Golebiewski, M., Sullivan, A., Yan, H., Hannah, N., Franklin, C., Sun, Z., Vohralik, P., Watterson, I., Zhou, X., Fiedler, R., Collier, M., Ma, Y., Noonan, J., Stevens, L., Uhe, P., Zhu, H., Griffies, S., Hill, R., Harris, C., Puri, K., 2013. The ACCESS Coupled Model: Description, Control Climate and Evaluation. Aust. Meteorol. Ocean. 63, 41–64, https://doi.org/10.22499/2.6301.004

Block, P.J., Strzepek, K., Rajagopalan, B., 2007. Integrated management of the Blue Nile Basin in Ethiopia: Hydropower and irrigation modeling. IFPRI Discussion Paper 00700. Available online at https://www.ifpri.org/cdmref/p15738coll2/id/38883/filename/38884.pdf (last access: 14 Jan 2021)

Chan, S.K., Bindlish, R., O'Neill, P.E., Njoku, E., Jackson, T., Colliander, A., Chen, F., Burgin, M., Dunbar, S., Piepmeier, J., Yueh, S., Entekhabi, D., Cosh, M.H., Caldwell, T., Walker, J., Wu, X., Berg, A., Rowlandson, T., Pacheco, A., McNairn, H., Thibeault, M., Martínez-Fernández, J., González-Zamora, Á., Seyfried, M., Bosch, D., Starks, P., Goodrich, D., Prueger, J., Palecki, M., Small, E.E., Zreda, M., Calvet, J.-C., Crow, W.T., Kerr, Y., 2016. Assessment of the SMAP Passive Soil Moisture Product. IEEE Trans. Geosci. Remote Sens. 54, 4994–5007. https://doi.org/10.1109/TGRS.2016.2561938

Crow, W. T., Berg, A. A., Cosh, M. H., Loew, A., Mohanty, B. P., Panciera, R., Rosnay, P., Ryu, D., Walker, J. P., 2012. Upscaling sparse ground-based soil moisture observations for the validation of coarse-resolution satellite soil moisture products. Rev. Geophys. 50. https://doi.org/10.1029/2011RG000372

Decker, M., 2015. Development and evaluation of a new soil moisture and runoff parameterization for the CABLE LSM including subgrid-scale processes. J. Adv. Model. Earth Syst. 7, 1788–1809. https://doi.org/10.1002/2015MS000507

Derksen, C., Toose, P., Rees, A., Wang, L., English, M., Walker, A., Sturm, M., 2010. Development of a tundra-specific snow water equivalent retrieval algorithm for satellite passive microwave data. Remote Sens. Environ. 114, 1699–1709. https://doi.org/10.1016/j.rse.2010.02.019

Dorigo, W., Wagner, W., Albergel, C., Albrecht, F., Balsamo, G., Brocca, L., Chung, D., Ertl, M., Forkel, M., Gruber, A., Haas, E., Hamer, P.D., Hirschi, M., Ikonen, J., de Jeu, R., Kidd, R., Lahoz, W., Liu, Y.Y., Miralles, D., Mistelbauer, T., Nicolai-Shaw, N., Parinussa, R., Pratola, C., Reimer, C., van der Schalie, R., Seneviratne, S.I., Smolander, T., Lecomte, P., 2017. ESA CCI Soil Moisture for improved Earth system understanding: State-of-the art and future directions. Remote Sens. Environ. 203, 185–215. https://doi.org/10.1016/j.rse.2017.07.001

Entekhabi, D., Njoku, E.G., O’Neill, P.E., Kellogg, K.H., Crow, W.T., Edelstein, W.N., Entin, J.K., Goodman, S.D., Jackson, T.J., Johnson, J., Kimball, J., Piepmeier, J.R., Koster, R.D., Martin, N., McDonald, K.C., Moghaddam, M., Moran, S., Reichle, R., Shi, J.C., Spencer, M.W., Thurman, S.W., Tsang, L., Zyl, J.V., 2010. The Soil Moisture Active Passive (SMAP) Mission. Proc. IEEE 98, 704–716. https://doi.org/10.1109/JPROC.2010.2043918

Flechtner, F., Neumayer, K.-H., Dahle, C., Dobslaw, H., Fagiolini, E., Raimondo, J.-C., Güntner, A., 2016. What Can be Expected from the GRACE-FO Laser Ranging Interferometer for Earth Science Applications? Surv. Geophys. 37, 453–470. https://doi.org/10.1007/s10712-015-9338-y

Girotto, M., De Lannoy, G.J.M., Reichle, R.H., Rodell, M., Draper, C., Bhanja, S.N., Mukherjee, A., 2017. Benefits and pitfalls of GRACE data assimilation: A case study of terrestrial water storage depletion in India. Geophys. Res. Lett. 44, 4107–4115. https://doi.org/10.1002/2017GL072994

Haddeland, I., Heinke, J., Biemans, H., Eisner, S., Flörke, M., Hanasaki, N., Konzmann, M., Ludwig, F., Masaki, Y., Schewe, J., Stacke, T., Tessler, Z.D., Wada, Y., Wisser, D., 2014. Global water resources affected by human interventions and climate change. PNAS 111, 3251–3256. https://doi.org/10.1073/pnas.1222475110

Hansen, P.C., O'Leary, D.P., 1993. The Use of the L-Curve in the Regularization of Discrete Ill-Posed Problems. SIAM J. Sci. Comput. 14, 1487–1503. https://doi.org/10.1137/0914086

Hersbach, H. and Dee, D.: ERA5 reanalysis is in production, ECMWF Newsletter, Vol. 147, p. 7, available at: https://www.ecmwf.int/en/newsletter/147/news/era5-reanalysis-production (last access: 3 June 2020), 2016.

Huntington, T.G., 2006. Evidence for intensification of the global water cycle: Review and synthesis. J. Hydrol. 319, 83–95. https://doi.org/10.1016/j.jhydrol.2005.07.003

Issa, I.E., Al-Ansari, N., Knutsson, S., 2013. Sedimentation and new operational curves for Mosul Dam, Iraq. Hydrol. Sci. J. 58, 1456–1466. https://doi.org/10.1080/02626667.2013.789138

Li, B., Rodell, M., Kumar, S., Beaudoing, H.K., Getirana, A., Zaitchik, B.F., Goncalves, L.G. de, Cossetin, C., Bhanja, S., Mukherjee, A., Tian, S., Tangdamrongsub, N., Long, D., Nanteza, J., Lee, J., Policelli, F., Goni, I.B., Daira, D., Bila, M., Lannoy, G. de, Mocko, D., Steele-Dunne, S.C., Save, H., Bettadpur, S., 2019. Global GRACE Data Assimilation for Groundwater and Drought Monitoring: Advances and Challenges. Water Resour. Res. 55, 7564–7586. https://doi.org/10.1029/2018WR024618

Long, D., Chen, X., Scanlon, B.R., Wada, Y., Hong, Y., Singh, V.P., Chen, Y., Wang, C., Han, Z., Yang, W., 2016. Have GRACE satellites overestimated groundwater depletion in the Northwest India Aquifer? Sci. Rep. 6, 24398. https://doi.org/10.1038/srep24398

Lu, J., Sun, G., McNulty, S.G., Amatya, D.M., 2005. A Comparison of Six Potential Evapotranspiration Methods for Regional Use in the Southeastern United States. JAWRA 41, 621–633. https://doi.org/10.1111/j.1752-1688.2005.tb03759.x

Luojus, K., Pulliainen, J., Takala, M., Moisander, M., Cohen, J., Ikonen, J., Lemmetyinen, J., 2017a: Copernicus Global Land Operations "Cryosphere and Water", preliminary quality assessment report, snow water equivalent 5km northern hemisphere version 1. Technical report issue I1.01. Available online at https://land.copernicus.eu/global/sites/cgls.vito.be/files/products/CGLOPS2_QAR_SWE-NH-5km-V1_I1.01.pdf (last access: 25 June 2020)

Luojus, K., Pulliainen, J., Moisander, M., Takala, M., Cohen, J., Lemmetyinen, J., 2017b: Copernicus Global Land Operations "Cryosphere and Water", product user manual, snow water equivalent 5km northern hemisphere version 1. Technical report issue I1.02. Available online at https://land.copernicus.eu/global/sites/cgls.vito.be/files/products/CGLOPS2_PUM_SWE-NH-5km-V1_I1.02.pdf (last access: 25 June 2020).

McNairn, H., Merzouki, A., Pacheco, A., Fitzmaurice, J., 2012. Monitoring Soil Moisture to Support Risk Reduction for the Agriculture Sector Using RADARSAT-2. IEEE J. Sel. Top. Appl. Earth Obs. Remote Sens. 5, 824–834. https://doi.org/10.1109/JSTARS.2012.2192416

Miller, B., Sweigart, E., 2019: How Countries Manage Water: Argentina. Americas Quarterly. Available online at: https://www.americasquarterly.org/article/how-countries-manage-water-argentina/ (last accessed 23 June 2020).

Miro, M.E., Famiglietti, J.S., 2018. Downscaling GRACE Remote Sensing Datasets to High-Resolution Groundwater Storage Change Maps of California's Central Valley. Remote Sens. 10, 143. https://doi.org/10.3390/rs10010143

Mueller, N., Lewis, A., Roberts, D., Ring, S., Melrose, R., Sixsmith, J., Lymburner, L., McIntyre, A., Tan, P., Curnow, S., Ip, A., 2016. Water observations from space: Mapping surface water from 25years of Landsat imagery across Australia. Remote. Sens. Environ. 174, 341–352. https://doi.org/10.1016/j.rse.2015.11.003

National Academies of Sciences, Engineering, and Medicine. 2018.Thriving on Our Changing Planet: A Decadal Strategy for Earth Observation from Space. Washington, DC: The National Academies Press. https://doi.org.10.17226/24938.

Peng, J., Loew, A., Merlin, O., Verhoest, N.E.C., 2017. A review of spatial downscaling of satellite remotely sensed soil moisture. Rev. Geophys. 55, 341–366. https://doi.org/10.1002/2016RG000543

Quiring, S.M., 2009. Developing Objective Operational Definitions for Monitoring Drought. J. Appl. Meteor. Climatol. 48, 1217–1229. https://doi.org/10.1175/2009JAMC2088.1

Reichle, R.H., De Lannoy, G.J.M., Liu, Q., Ardizzone, J.V., Colliander, A., Conaty, A., Crow, W., Jackson, T.J., Jones, L.A., Kimball, J.S., Koster, R.D., Mahanama, S.P., Smith, E.B., Berg, A., Bircher, S., Bosch, D., Caldwell, T.G., Cosh, M., González-Zamora, Á., Holifield Collins, C.D., Jensen, K.H., Livingston, S., Lopez-Baeza, E., Martínez-Fernández, J., McNairn, H., Moghaddam, M., Pacheco, A., Pellarin, T., Prueger, J., Rowlandson, T., Seyfried, M., Starks, P., Su, Z., Thibeault, M., van der Velde, R., Walker, J., Wu, X., Zeng, Y., 2017. Assessment of the SMAP Level-4 Surface and Root-Zone Soil Moisture Product Using In Situ Measurements. J. Hydrometeor. 18, 2621–2645. https://doi.org/10.1175/JHM-D-17-0063.1

Reichle, R.H., Koster, R.D., 2004. Bias reduction in short records of satellite soil moisture. Geophys. Res. Lett. 31, L19501. https://doi.org/10.1029/2004GL020938

Rodell, M., Houser, P.R., Jambor, U., Gottschalck, J., Mitchell, K., Meng, C.-J., Arsenault, K., Cosgrove, B., Radakovich, J., Bosilovich, M., Entin, J.K., Walker, J.P., Lohmann, D., Toll, D., 2004. The Global Land Data Assimilation System. Bull. Amer. Meteor. Soc. 85, 381–394. https://doi.org/10.1175/BAMS-85-3-381

Rodell, M., Velicogna, I., Famiglietti, J.S., 2009. Satellite-based estimates of groundwater depletion in India. Nature 460, 999. https://doi.org/10.1038/nature08238

Rowlands, D.D., Luthcke, S.B., McCarthy, J.J., Klosko, S.M., Chinn, D.S., Lemoine, F.G., Boy, J.-P., Sabaka, T.J., 2010. Global mass flux solutions from GRACE: A comparison of parameter estimation strategies—Mass concentrations versus Stokes coefficients. J. Geophys. Res. Solid Earth 115. https://doi.org/10.1029/2009JB006546

Scanlon, B.R., Zhang, Z., Save, H., Sun, A.Y., Schmied, H.M., Beek, L.P.H. van, Wiese, D.N., Wada, Y., Long, D., Reedy, R.C., Longuevergne, L., Döll, P., Bierkens, M.F.P., 2018. Global models underestimate large decadal declining and rising water storage trends relative to GRACE satellite data. PNAS 201704665. https://doi.org/10.1073/pnas.1704665115

Sorg, A., Bolch, T., Stoffel, M., Solomina, O., Beniston, M., 2012. Climate change impacts on glaciers and runoff in Tien Shan (Central Asia). Nat. Clim. Change 2, 725–731. https://doi.org/10.1038/nclimate1592

Sutanudjaja, E.H., van Beek, L.P.H., de Jong, S.M., van Geer, F.C., Bierkens, M.F.P., 2011. Large-scale groundwater modeling using global datasets: a test case for the Rhine-Meuse basin. Hydrol. Earth Syst. Sci. 15, 2913–2935. https://doi.org/10.5194/hess-15-2913-2011

Sutanudjaja, E.H., van Beek, R., Wanders, N., Wada, Y., Bosmans, J.H.C., Drost, N., van der Ent, R.J., de Graaf, I.E.M., Hoch, J.M., de Jong, K., Karssenberg, D., López López, P., Peßenteiner, S., Schmitz, O., Straatsma, M.W., Vannametee, E., Wisser, D., Bierkens, M.F.P., 2018. PCR-GLOBWB 2: a 5 arcmin global hydrological and water resources model. Geosci. Model Dev. 11, 2429–2453. https://doi.org/10.5194/gmd-11-2429-2018

Syed, T.H., Famiglietti, J.S., Chen, J., Rodell, M., Seneviratne, S.I., Viterbo, P., Wilson, C.R., 2005. Total basin discharge for the Amazon and Mississippi River basins from GRACE and a land-atmosphere water balance. Geophys. Res. Lett. 32, L24404. https://doi.org/10.1029/2005GL024851

Tamisiea, M.E., Mitrovica, J.X., Davis, J.L., 2007. GRACE Gravity Data Constrain Ancient Ice Geometries and Continental Dynamics over Laurentia. Science 316, 881–883. https://doi.org/10.1126/science.1137157

Tangdamrongsub, N., Ditmar, P.G., Steele-Dunne, S.C., Gunter, B.C., Sutanudjaja, E.H., 2016. Assessing total water storage and identifying flood events over Tonlé Sap basin in Cambodia using GRACE and MODIS satellite observations combined with hydrological models. Remote. Sens. Environ. 181, 162–173. https://doi.org/10.1016/j.rse.2016.03.030

Tangdamrongsub, N., Han, S.-C., Decker, M., Yeo, I.-Y., Kim, H., 2018. On the use of the GRACE normal equation of inter-satellite tracking data for estimation of soil moisture and groundwater in Australia. Hydrol. Earth Syst. Sci. 22, 1811–1829. https://doi.org/10.5194/hess-22-1811-2018

Tangdamrongsub, N., Hwang, C., Shum, C.K., Wang, L., 2012. Regional surface mass anomalies from GRACE KBR measurements: Application of L-curve regularization and a priori hydrological knowledge. J. Geophys. Res. Solid Earth 117. https://doi.org/10.1029/2012JB009310

Tangdamrongsub, N., Šprlák, M., 2021. The Assessment of Hydrologic- and Flood-Induced Land Deformation in Data-Sparse Regions Using GRACE/GRACE-FO Data Assimilation. Remote Sens. 13, 235. https://doi.org/10.3390/rs13020235

Tapley, B.D., Bettadpur, S., Ries, J.C., Thompson, P.F., Watkins, M.M., 2004. GRACE Measurements of Mass Variability in the Earth System. Science 305, 503–505. https://doi.org/10.1126/science.1099192

Tapley, B.D., Watkins, M.M., Flechtner, F., Reigber, C., Bettadpur, S., Rodell, M., Sasgen, I., Famiglietti, J.S., Landerer, F.W., Chambers, D.P., Reager, J.T., Gardner, A.S., Save, H., Ivins, E.R., Swenson, S.C., Boening, C., Dahle, C., Wiese, D.N., Dobslaw, H., Tamisiea, M.E., Velicogna, I., 2019. Contributions of GRACE to understanding climate change. Nat. Clim. Change 9, 358. https://doi.org/10.1038/s41558-019-0456-2

van Dijk, A.I.J.M., Schellekens, J., Yebra, M., Beck, H.E., Renzullo, L.J., Weerts, A., Donchyts, G., 2018. Global 5 km resolution estimates of secondary evaporation including irrigation through satellite data assimilation. Hydrol. Earth Syst. Sci. 22, 4959–4980. https://doi.org/10.5194/hess-22-4959-2018

Wiese, D. N., Landerer, F. W., Watkins, M. M. (2016), Quantifying and reducing leakage errors in the JPL RL05M GRACE mascon solution, Water Resour. Res., 52, 7490–7502, doi:10.1002/2016WR019344.

Xia, Y., Mitchell, K., Ek, M., Sheffield, J., Cosgrove, B., Wood, E., Luo, L., Alonge, C., Wei, H., Meng, J., Livneh, B., Lettenmaier, D., Koren, V., Duan, Q., Mo, K., Fan, Y., Mocko, D., 2012. Continental-scale water and energy flux analysis and validation for the North American Land Data Assimilation System project phase 2 (NLDAS-2): 1. Intercomparison and application of model products. J. Geophys. Res. Atmospheres 117. https://doi.org/10.1029/2011JD016048

Yin, W., Li, T., Zheng, W., Hu, L., Han, S.-C., Tangdamrongsub, N., Šprlák, M., Huang, Z., 2020. Improving regional groundwater storage estimates from GRACE and global hydrological models over Tasmania, Australia. Hydrogeol J. https://doi.org/10.1007/s10040-020-02157-3

Yin, W., Hu, L., Zhang, M., Wang, J., Han, S.-C., 2018. Statistical Downscaling of GRACE-Derived Groundwater Storage Using ET Data in the North China Plain. J. Geophys. Res. Atmospheres 123, 5973–5987. https://doi.org/10.1029/2017JD027468

Table 1: Characteristics and data access of groundwater networks used in the evaluation

Regions	Groundwater networks	Data access
South East CONUS	The U.S. Geological Survey (USGS) groundwater watch	https://groundwaterwatch.usgs.gov/usgsgwnetworks.asp (last access: 7 July 2020)
Rhine	Three different networks are used, 1) Ministerium für Klimaschutz, Umwelt, Landwirtschaft, Natur- und Verbraucherschutz des Landes Nordrhein-Westfalen, 2) Bayerisches Landesamt für Umwelt, and 3) Portail national d'Accès aux Donnéessur les Eaux Souterraines	Data access is given in Tangdamrongsub et al. (2015)
North West India	The Central Ground Water Board of India	http://cgwb.gov.in/GW-data-access.html (last access: 7 July 2020)
North China Plain	The Ministry of Water Resources of China (MWRC)	http://www.mwr.gov.cn/english (last access: 6 July 2020)
Victoria	The Australian Bureau of Meteorology through the Australian Groundwater Explorer	http://www.bom.gov.au/water/groundwater/explorer/map.shtml (last access: 7 July 2020)

Table 2: Regional-average correlation values of the ∆GWS estimates computed from a priori knowledge (i.e., model simulation) and the LSC solutions, with respect to the in situ groundwater measurements. The overall (average) correlation values of each case are also given.

Regions	**A prior knowledge**			**LSC solution**		
	Ens-Mean	**CABLE**	**PCR-GLOWB**	**Ens-Mean**	**CABLE**	**PCR-GLOBWB**
South East CONUS	0.86	0.76	0.90	0.89	0.84	0.91
Rhine	0.46	-0.10	0.91	0.51	0.09	0.93
North West India	0.78	0.46	0.79	0.86	0.48	0.82
North China Plain	0.70	0.58	0.56	0.86	0.64	0.85
Victoria	0.57	0.69	0.33	0.86	0.76	0.64
Average	0.67	0.48	0.70	0.80	0.56	0.83

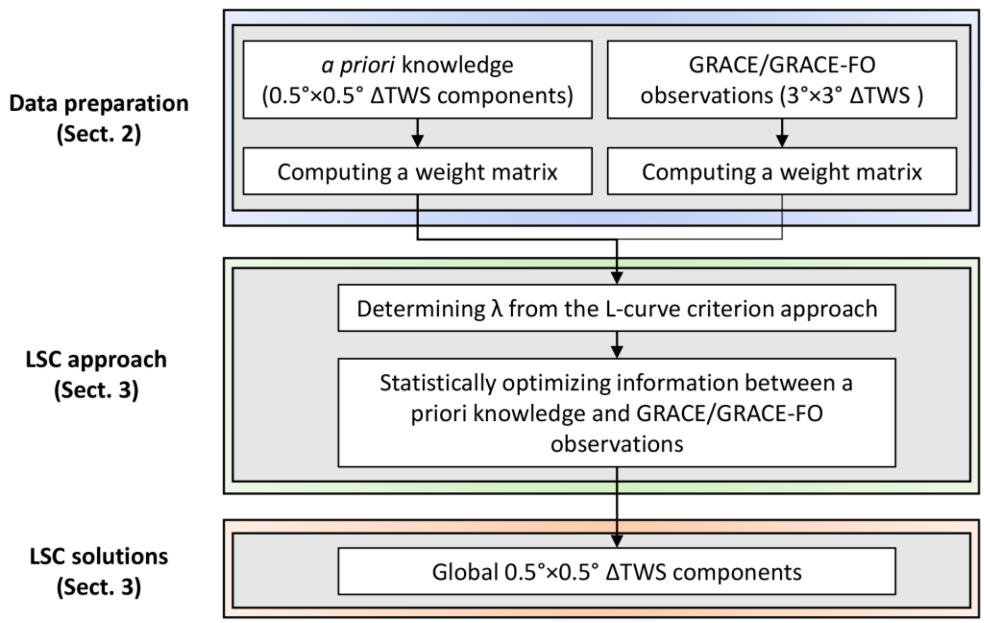

Figure 1: Data processing diagram of the LSC approach. Section number (Sect.) indicates the section of this article where comprehensive processing details can be found.

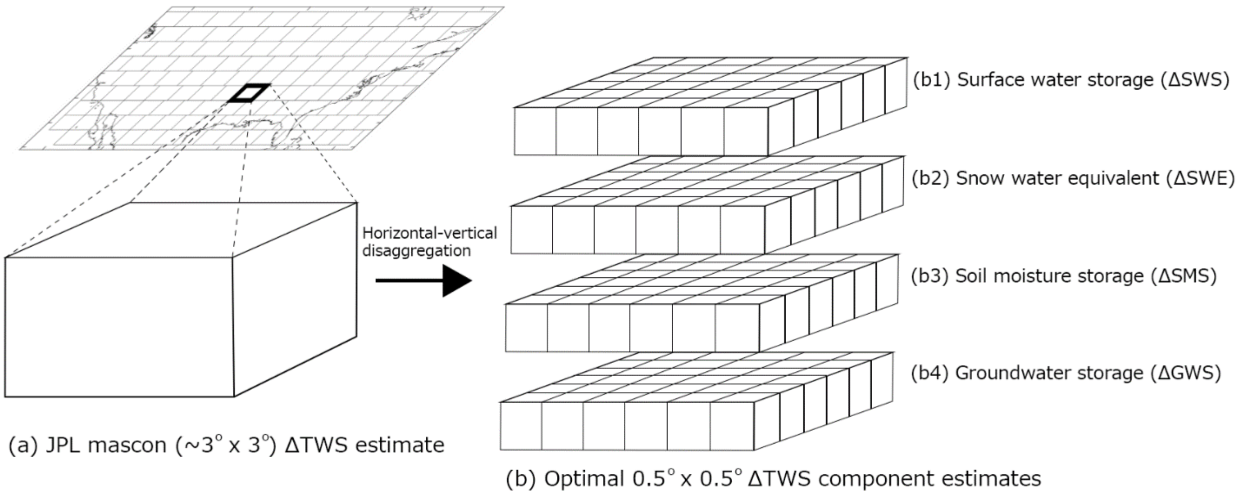

Figure 2: The concept of horizontal-vertical disaggregation of 3°×3° GRACE JPL mascon-derived ΔTWS to four different ΔTWS components (e.g., ΔSWS, ΔSWE, ΔSMS, and ΔGWS) at 0.5°×0.5° spatial resolution.

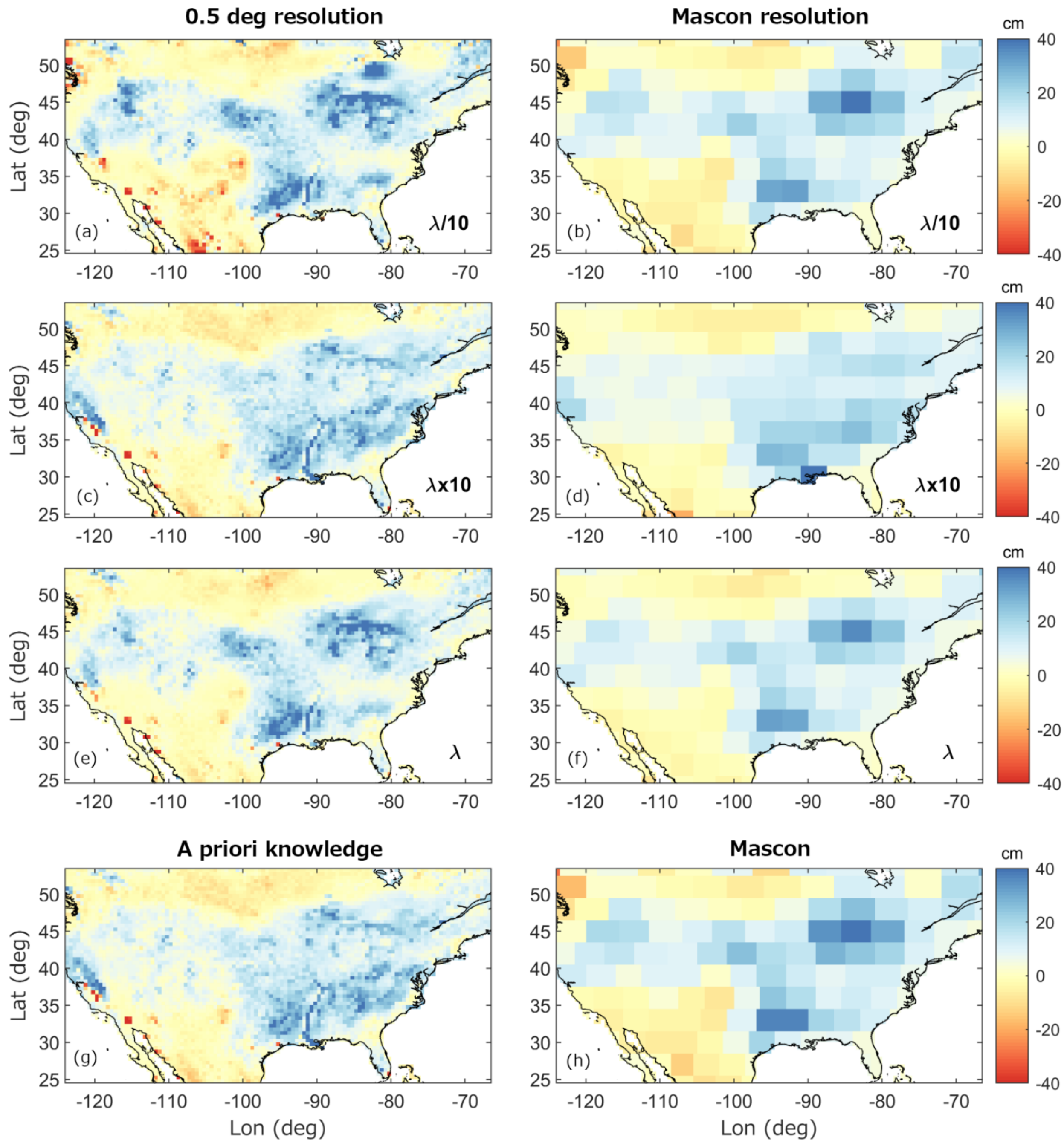

Figure 3: The EnsMean-based ΔTWS estimates as a function of λ values, (a, b) optimal λ divided by 10, (c, d) optimal λ multiplied by 10, and (e, f) optimal λ, The May 2019 solution is shown here. The left panels (a, c, e) show the LSC solutions, while the right right panels (b, d, f) illustrate the same result but spatially averaged to mascon spatial resolution (i.e., upscaling from 0.5°×0.5° to ~3°×3°). The (ensemble-mean) prior knowledge and GRACE JPL mascon solution of May 2019 are also shown, in (g) and (h), respectively.

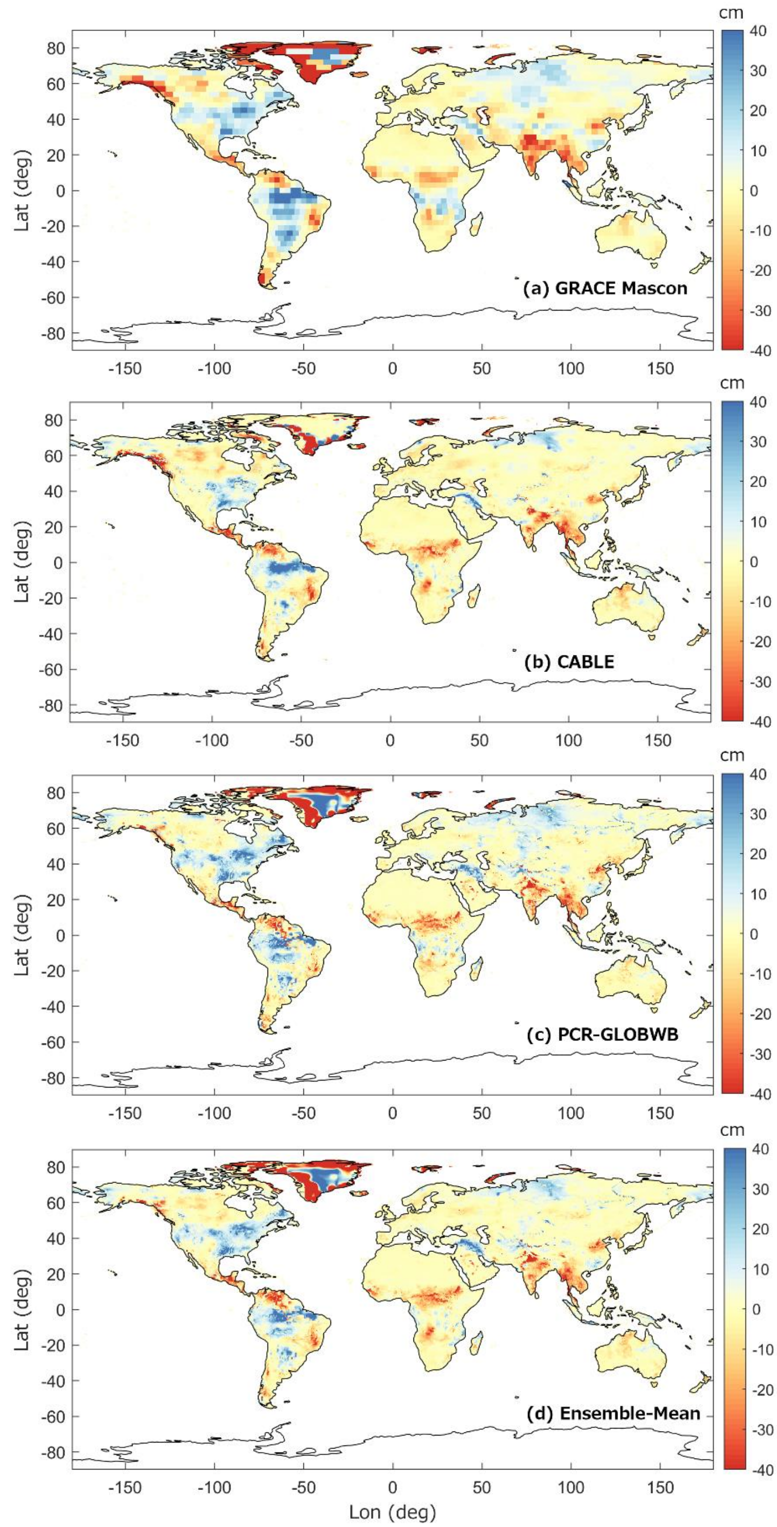

Figure 4: Global ΔTWS estimates of May 2019 obtained from (a) GRACE JPL mascon, and LSC solutions estimated based on different *a priori* knowledge, (b) CABLE, (c) PCR-GLOBWB, and (d) ensemble-mean models.

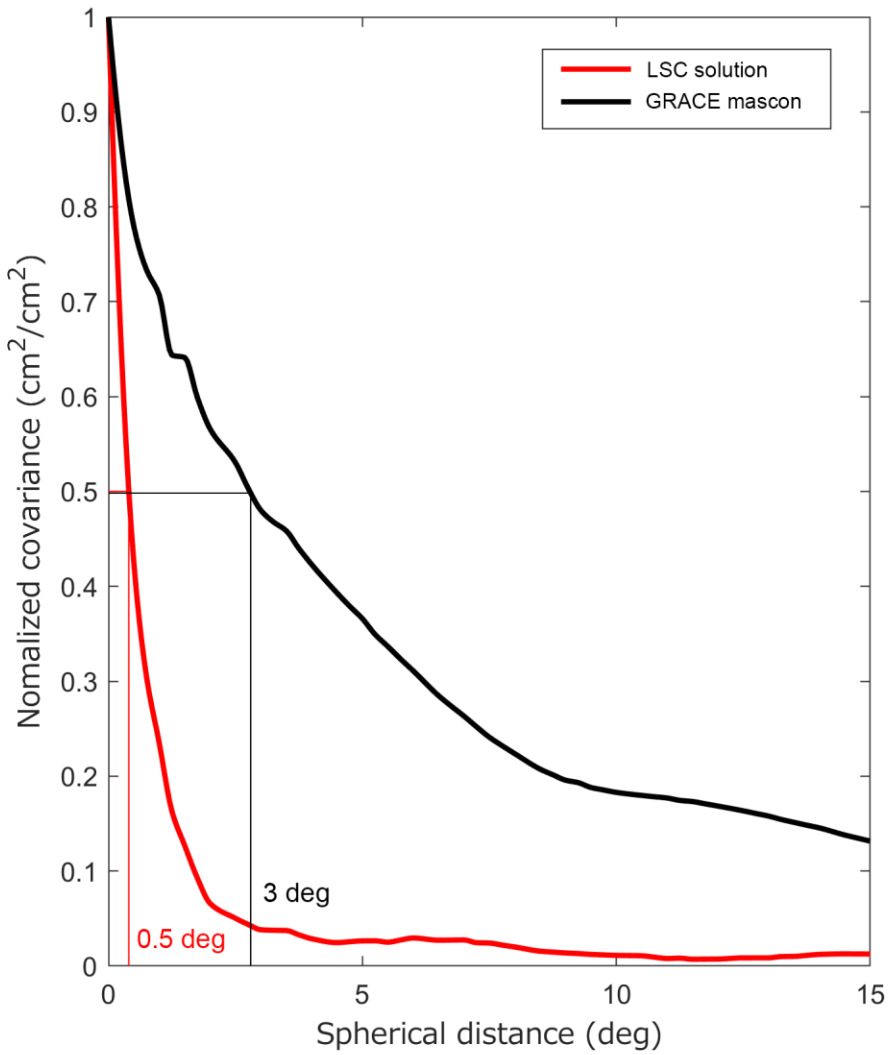

Figure 5: Normalized empirical covariances computed from the ΔTWS estimates of the 3°×3° GRACE mascon and the 0.5°×0.5° EnsMean-based solution. The result of the May 2019 solution is shown here. The spatial resolution is estimated as a spherical distance (degree), where the variance (normalized covariance value equal to one) decreases by half. The GRACE mascon estimate reflects its intrinsic spatial resolution (3°), while the LSC estimate shows the same resolution as a priori knowledge (0.5°). The same behavior is also observed in the CABLE-based and PCR-GLOBWB-based solutions and all monthly solutions.

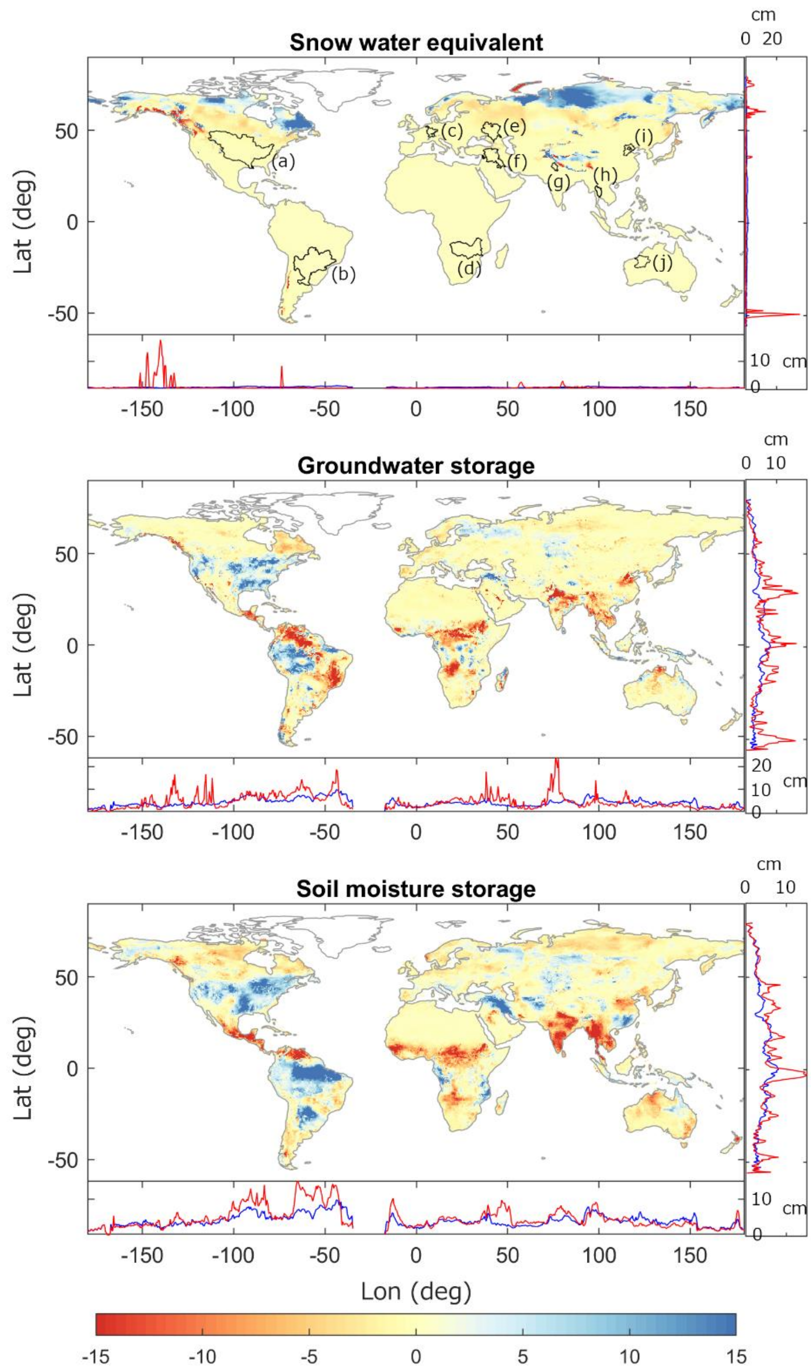

Figure 6: The ΔSWE (top), ΔGWS (middle), and ΔSMS (bottom) of May 2019 estimated from the EnsMean-based solution. The RMSs calculated along latitude and longitude axes are shown in each figure (red). For comparison, the RMSs of a prior knowledge (ensemble-mean mdoel) are also shown (blue). The polygons shown in ΔSWE (top) are the river basin boundaries used in Fig. 7's discussion. The displayed river basins are (a) Mississippi, (b) Parana, (c) Rhine, (d) Zambezi, (e) Don, (f) Tigrid-Euphrates, (g) North West India, (h) Chao Phraya, (i) North China Plain, and (j) Sandy Desert.

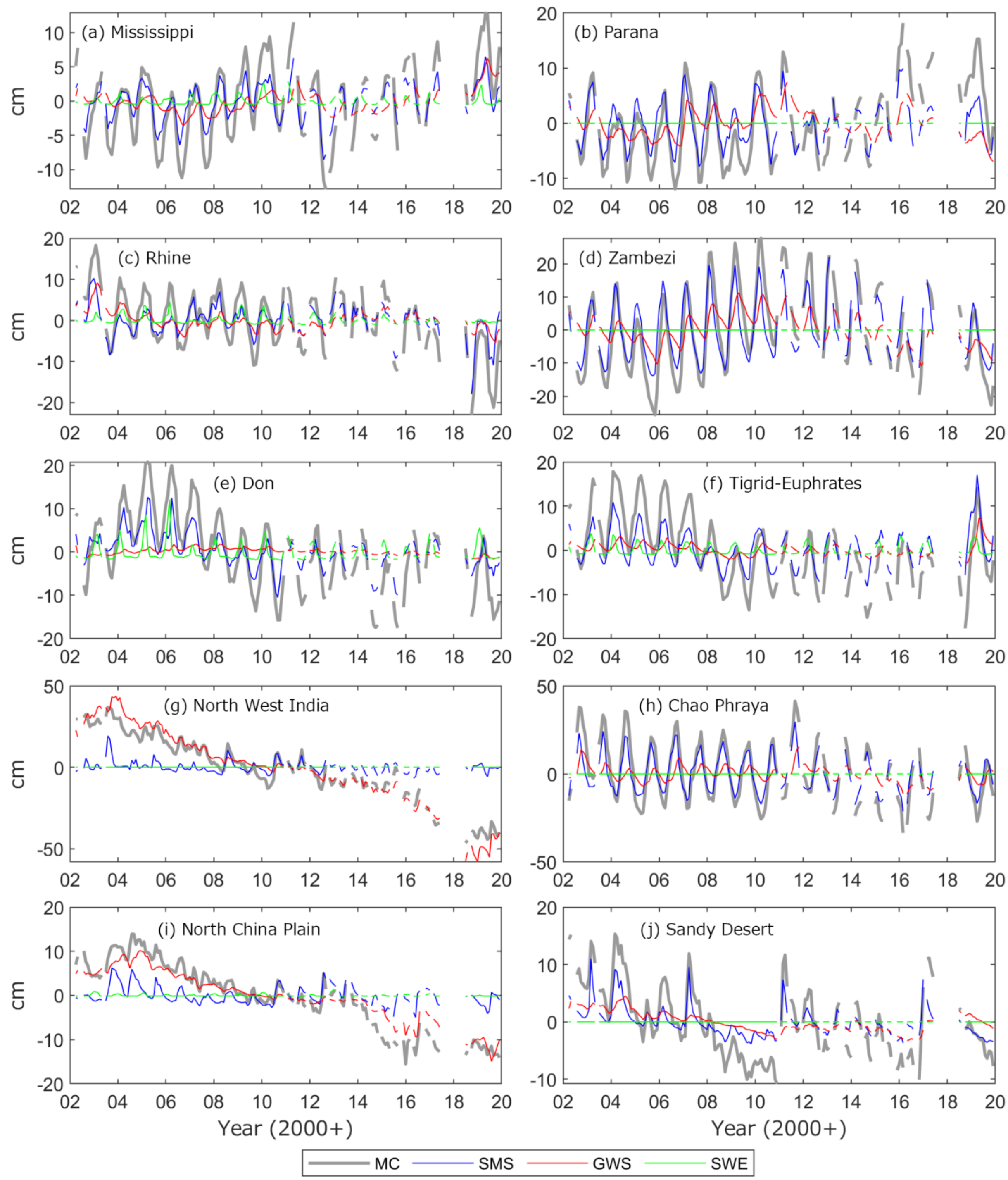

Figure 7: Basin-averaged time series of ΔSMS, ΔGWS, and ΔSWE estimates computed from the Ensmean-based solution, in (a) Mississippi, (b) Parana, (c) Rhine, (d) Zambezi, (e) Don, (f) Tigrid-Euphrates, (g) North West India, (h) Chao Phraya, (i) North China Plain, and (j) Sandy Desert. The time series of GRACE mascon derived ΔTWS (MC) is also shown. The river basin's boundaries can be found in Fig. 6.

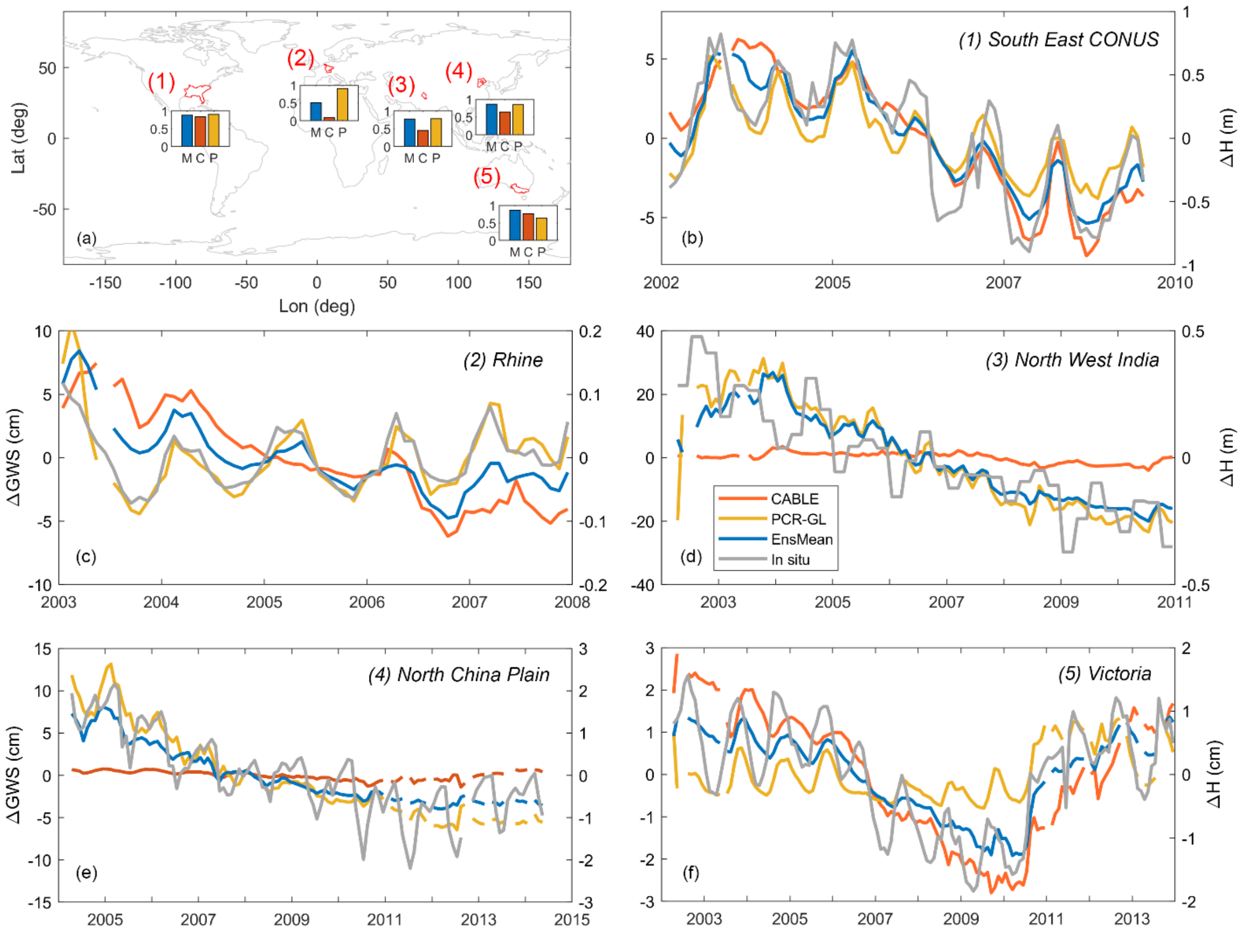

Figure 8: (a) Spearman's correlation values between in situ groundwater measurements and LSC solutions associated with different *a priori* knowledge, CABLE (C), PCR-GLOBWB (P), and ensemble-mean (M) models in five different regions, (1) South East CONUS, (2) Rhine, (3) North West India, (4) North China Plain, and (5) Victoria. (b – f) The time series of the ΔGWS estimates and groundwater level anomalies (ΔH) in the five discussed regions. Note that the scales of horizontal (time) and vertical axes are different for different regions.

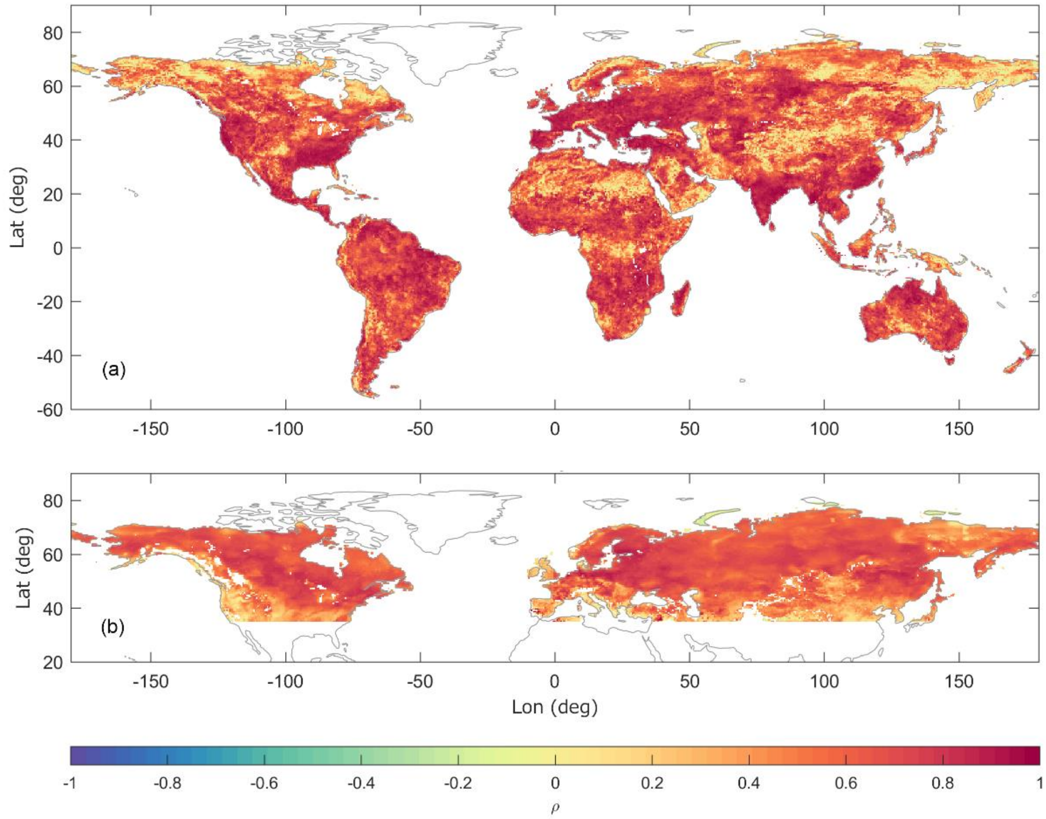

Figure 9: Correlations (ρ) of (a) ΔSMS and (b) ΔSWE computed from the EnsMean-based solution with respect to the SMAP Level 4 data and CGLS-SWE products, respectively.

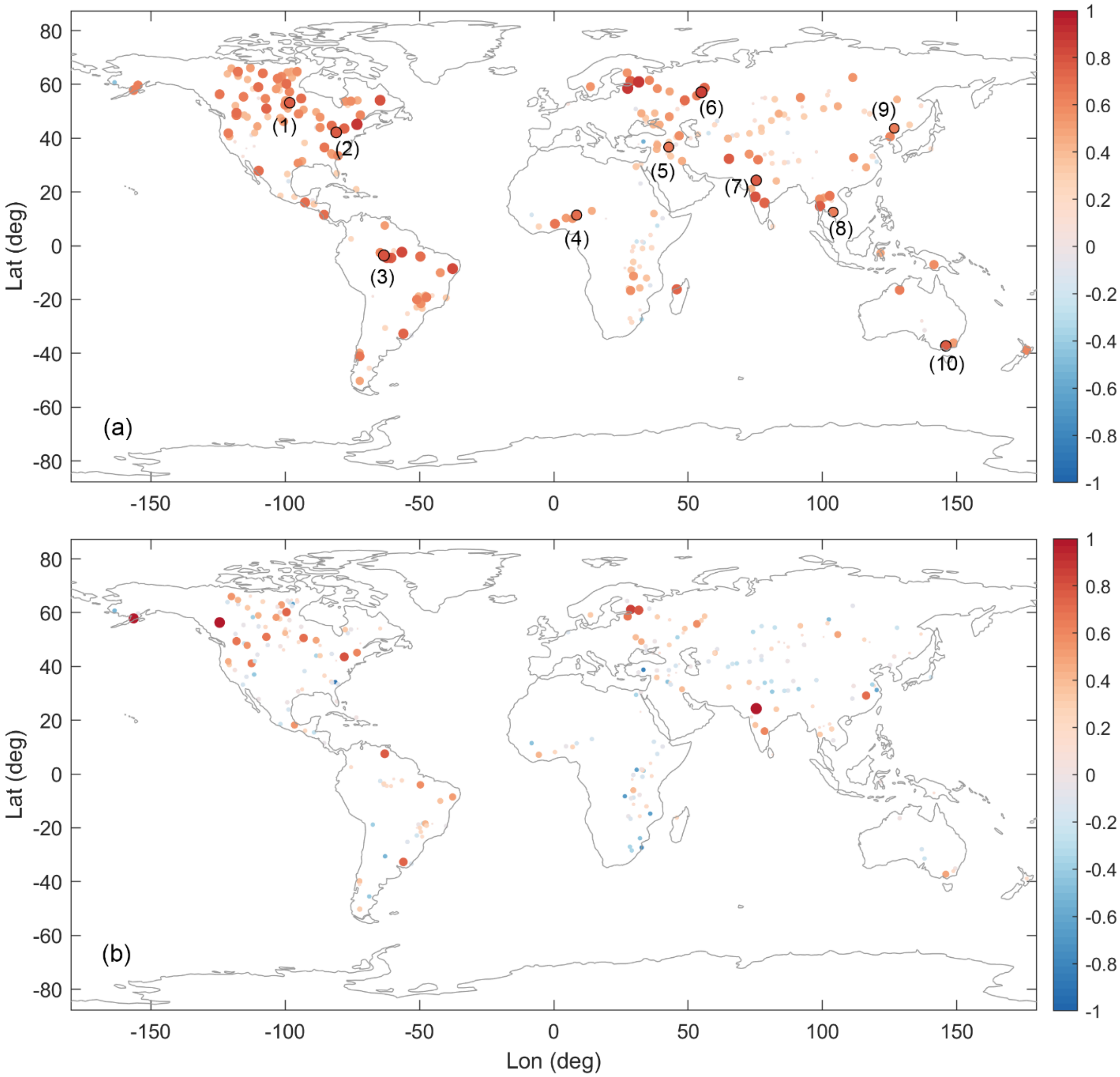

Figure 10: (a) Correlations between the ΔSWS estimate and altimetry-derived water level anomaly. (b) The correlation differences computed by subtracting correlation values of a priori knowledge (PCR-GLOBWB) from the LSC PCR-GLOBWB-based estimates, i.e., ρ_{LSC} minus ρ_{prior}. The positive and negative impacts of including GRACE mascon solution (in the LSC approarch) are indicated by hot and cold colors, respectively. For visualization, the radius of the scatter plot (circle) increases with increasing correlation value. The scatter plots with black circumferences (see a – j in (a)) are the lakes or reservoirs used in Fig. 11's discussion. The selected lakes and reservoirs are (1) Lake Winnipeg, (2) Lake Erie, (3) Lake Lago Piorini, (4) Tiga Reservoir, (5) Mosul Reservoir, (6) Votkinskoye Reservoir, (7) Gandhi Sagar Reservoir, (8) Tonlé Sap Lake, (9) Song Hua Lake, and (10) Lake Eildon.

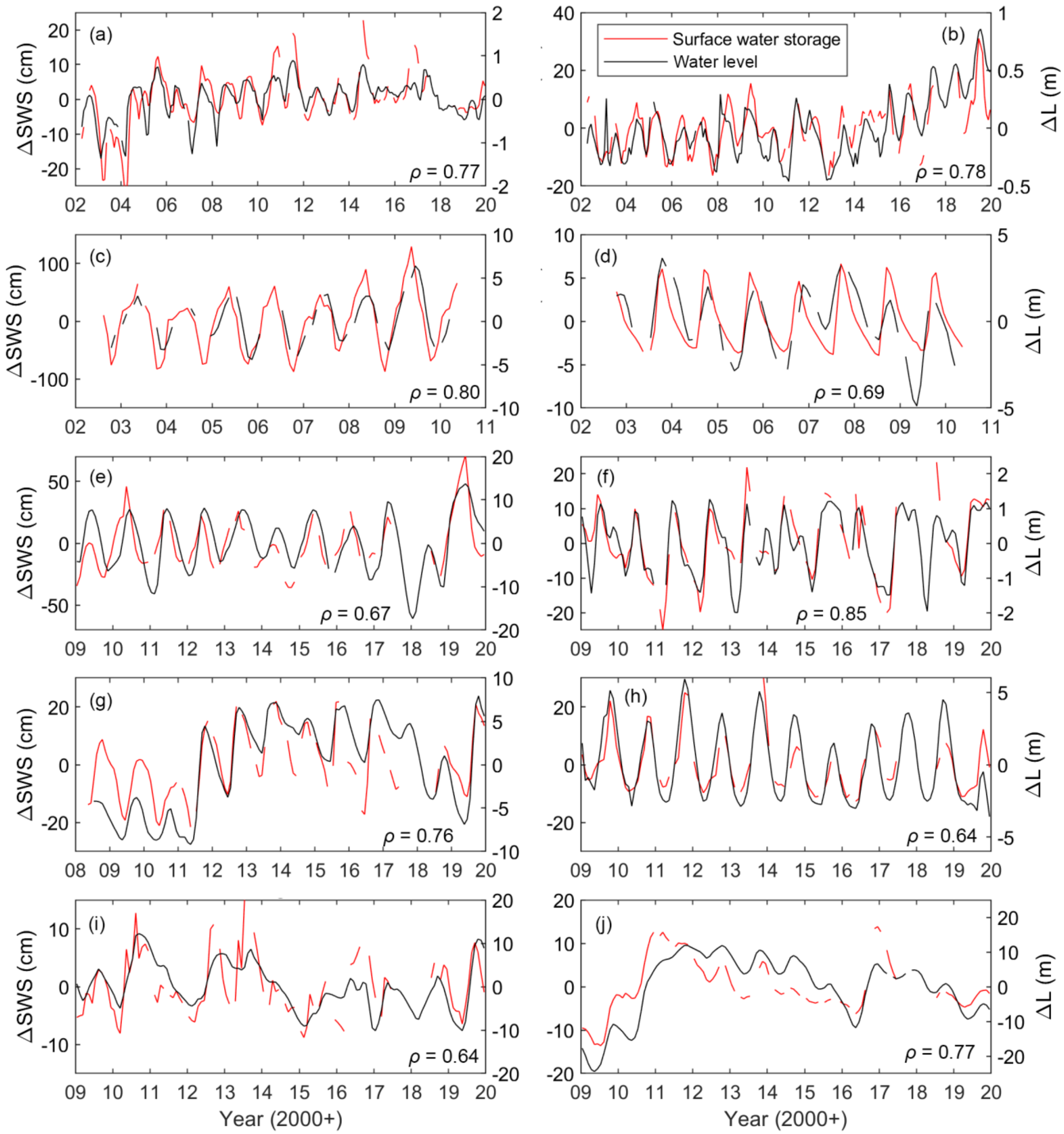

Figure 11: The LSC ΔSWS estimates and water level anomalies (ΔL) of (a) Lake Winnipeg, (b) Lake Erie, (c) Lake Lago Piorini, (d) Tiga Reservoir, (e) Mosul Reservoir, (f) Votkinskoye Reservoir, (g) Gandhi Sagar Reservoir, (h) Tonlé Sap Lake, (i) Song Hua Lake, and (j) Lake Eildon. The PCR-GLOBWB-based solution is used in the evaluation regarding the availability of the ΔSWS component. The correlation (ρ) value between ΔSWS and ΔL is also given in each subplot. Note that the scales of horizontal and vertical axes are different for different lakes/reservoirs.

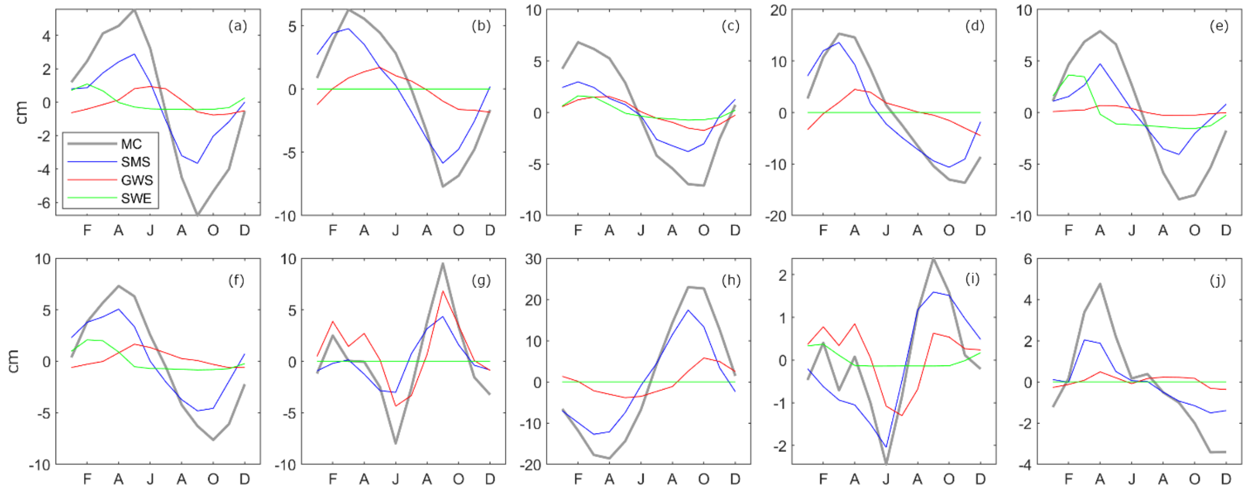

Figure S1: Monthly basin-average ΔSMS, ΔGWS, and ΔSWE estimates (similar to Fig. 7) from the (EnsMean-based) LSC solution in (a) Mississippi, (b) Parana, (c) Rhine, (d) Zambezi, (e) Don, (f) Tigrid-Euphrates, (g) North West India, (h) Chao Phraya, (i) North China Plain, and (j) Sandy Desert. The GRACE mascon derived ΔTWS (MC) is also shown.

Figure S2: Yearly precipitation obtained from the ERA5 product over (a) Lake Winnipeg, (b) Lake Erie, (c) Lake Lago Piorini, (d) Tiga Reservoir, (e) Mosul Reservoir, (f) Votkinskoye Reservoir, (g) Gandhi Sagar Reservoir, (h) Tonlé Sap Lake, (i) Song Hua Lake, and (j) Lake Eildon between 2002 and 2019.

Figure S3: Yearly average temperature obtained from the ERA5 product over (a) Lake Winnipeg, (b) Lake Erie, (c) Lake Lago Piorini, (d) Tiga Reservoir, (e) Mosul Reservoir, (f) Votkinskoye Reservoir, (g) Gandhi Sagar Reservoir, (h) Tonlé Sap Lake, (i) Song Hua Lake, and (j) Lake Eildon between 2002 and 2019.